NMR structure of the mature dimer initiation complex of HIV-1 genomic RNA

Anwer Mujeeb[a], Tristram G. Parslow[b,c,*], Ali Zarrinpar[d], Chandreyee Das[a], Thomas L. James[a]

[a]*Department of Pharmaceutical Chemistry, University of California at San Francisco, San Francisco, CA 94143, USA*
[b]*Department of Pathology, Box 0506, University of California at San Francisco, San Francisco, CA 94143, USA*
[c]*Department of Microbiology and Immunology, University of California at San Francisco, San Francisco, CA 94143, USA*
[d]*Department of Biochemistry, University of California at San Francisco, San Francisco, CA 94143, USA*

Received 9 August 1999

Abstract The two identical genomic RNA strands inside each HIV-1 viral particle are linked through homodimerization of an RNA stem-loop, termed SL1, near their 5′ ends. SL1 first dimerizes through a palindromic sequence in its loop, forming a transient kissing-loop complex which then refolds to a mature, linear duplex. We previously reported the NMR structure of a 23-base truncate of SL1 in kissing-dimer form, and here report the high-resolution structure of its linear isoform. This structure comprises three short duplex regions – derived from the central palindrome and two stem regions of each strand, respectively – separated by two bulges that each encompass three unpaired adenines flanking the palindromes. The stacking pattern of these adenines differs from that seen in the kissing-loop complex, and leads to greater colinear base stacking overall. Moreover, the mechanical distortion of the palindrome helix is reduced, and base pairs ruptured during formation of the kissing-loop complex are re-established, so that all potential Watson-Crick pairs are intact. These features together likely account for the greater thermodynamic stability of the mature dimer as compared to its kissing-loop precursor.

Key words: Dimerization; HIV-1 genome; NMR; RNA-RNA interaction; RNA structure; Packaging

1. Introduction

Retroviruses incorporate two copies of their single-stranded RNA genome into each viral particle ([1], and references therein). Within the particle, these RNAs exist as a non-covalent homodimer in which the two strands are aligned parallel and in register, associating most stably at a discrete region (called the dimer linkage site, DLS) near their 5′ ends. Because genomic dimerization is essential for maximal infectivity of a virus [2–4], the dimerization process offers a potential new target for antiretroviral therapeutics. Studies of genomic dimerization in the type 1 human immunodeficiency virus (HIV-1), using either synthetic RNAs or live viruses, indicate that the crucial first steps in dimer formation are mediated by a specific 35-nucleotide (nt) RNA stem-loop structure, termed SL1, whose location coincides with that of the DLS and whose loop includes a 6-nt palindrome ([4–7] and references therein). In many common strains of HIV-1, this palindrome has the sequence GCGCGC and is flanked by one 3′ and two 5′ purine residues (usually adenines); both the palindrome and the flanking purines are highly conserved (Fig. 1). Dimerization begins when the SL1 stem-loops of two genomic strands associate by Watson-Crick base-pairing of their loop palindromes, forming a transient kissing-loop complex. This complex is then believed to isomerize into a linear duplex, sometimes called the mature SL1 dimer initiation complex, in which the intrastrand base pairs of the stems have melted and reformed as interstrand pairs, creating a more stable linkage between the two strands. Isomerization of the dimer is catalyzed in vivo by the HIV-1 nucleocapsid protein [8], which binds specifically to SL1 [9].

We previously reported the NMR structure of the kissing-loop dimer formed by a 23-nt truncated derivative of SL1 RNA [10]. This derivative, called SL1Δ, includes all features of authentic SL1 that are needed for efficient dimerization, including the wild-type loop and distal stem sequences. We found that the two strands in the kissing-loop complex are linked not only by base-pairing between palindromes (which formed a bent minihelix discontinuous from the stem helices) but also by interstrand stacking interactions involving the flanking loop adenines. Those interactions create mechanical strains that induce partial melting of the distal G·C base pair in each of the two stem helices. We now report the structure of the SL1Δ dimer in its mature, linear form. Our findings confirm those recently described for another linear SL1 dimer of slightly different sequence [11] and provide additional details regarding its structural dynamics and the interactions that contribute to its stability.

2. Materials and methods

2.1. NMR sample preparation

The 23-nt SL1Δ RNA was synthesized enzymatically and purified as described [10]. NMR samples were prepared by dissolving the RNA at 300 μM in 10 mM sodium phosphate (pH 7.0), 20 mM NaCl; this was heated to 90°C for 2 min and then slowly cooled to room temperature. This protocol provided essentially pure RNA duplexes as determined by native polyacrylamide gel electrophoresis. For analysis of non-exchangeable protons, the same protocol was applied to a sample already lyophilized several times against D_2O.

2.2. NMR spectroscopy

All proton NMR experiments were performed at 600 MHz on a Varian Unityplus spectrometer, and were processed using NMRpipe and SPARKY software on a Silicon Graphics workstation. Two-dimensional (2D) NOE spectra with mixing times of 50, 200, and 400 ms in D_2O or water were collected at 25°C and 15°C, respectively, using essentially the same parameters described earlier [10]. Double-quantum-filtered COSY (dqfCOSY) and total correlated spectroscopy (TOCSY) studies were also performed as described [10].

*Corresponding author. Fax: (1) (415) 476-9672.
E-mail: parslow@cgl.ucsf.edu

PII: S0014-5793(99)01183-7

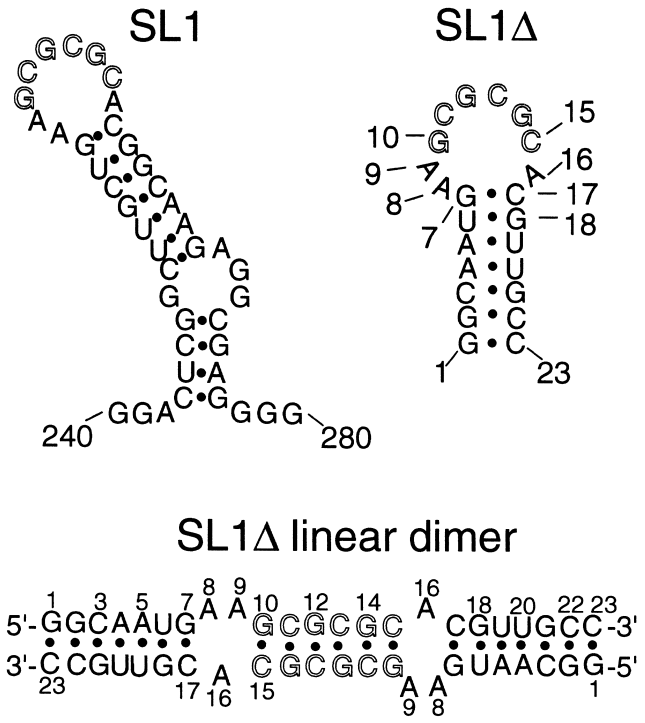

Fig. 1. Sequences and presumed secondary structures of the authentic RNA locus SL1 from HIV-1 strain LAI, and of its analog SL1Δ used in the present study. Residues in SL1 are numbered relative to the transcriptional start site. SL1Δ is shown in putative monomer (above) and linear dimer forms (below); for simplicity, references to stem and loop bases of SL1Δ in this report always refer to their conformations in the monomer.

One-dimensional ^{31}P NMR experiments were carried out in a 5-mm Shigemi NMR tube on a Bruker AMX 600 NMR spectrometer at 242.9 MHz ^{31}P frequency with a 70° pulse length, 12 000 Hz spectral width, a repetition time of 0.1 s, and 24 000 scans. There was no zero-filling during processing, but a 1-Hz exponential line broadening was applied prior to Fourier transformation. All ^{31}P spectra were referenced to the resonance from phosphate buffer, and processed using XWINNMR-1.0 software.

2.3. Extraction of distance restraints from NMR data

Structures were initially estimated using the DYANA 1.2 program with semi-quantitative upper and lower bounds on distance restraints. Resonance intensities were classified as strong, medium, weak or very weak, with upper bounds of 3.0, 4.0, 5.5, or 6.0Å assigned to these categories, respectively. Structures that best agreed with the NMR data were restraint-energy-minimized in AMBER 5.0, and then were used as starting structures in the program MARDIGRAS [12], which uses the complete relaxation matrix approach to calculate accurate interproton distance restraints from 2D NOE data. Assuming isotropic molecular motion, a correlation time of 8–10 ns was estimated for the molecule. MARDIGRAS calculations were carried out using 2D NOE data from mixing times of 50 and 400 ms, at correlation times of 8, 9, and 10 ns. The randmardi procedure [13] was applied during MARDIGRAS calculations to account for errors due to limitations in signal-to-noise and integration routines.

The program SYMM [14] was used to correct the intensities for partial relaxation effects arising from the 1.5-s delay time used in our 2D NOE experiments. This correction was performed prior to all MARDIGRAS calculations. Percentage error variations in the intensities on both sides of the diagonal were also calculated in SYMM and were later used as estimates of random error in the randmardi approach. Intensities that represented intra-sugar distances or involved H4′, H5′ or H5″ protons were excluded from the final set (Table 1).

Restraint bounds were constructed from six randmardi calculations at three correlation times for each of two mixing-time datasets. In each analysis, 50 cycles of MARDIGRAS calculations were performed. For each interproton distance, final bounds were assigned after discarding the longest and shortest 10% of values. A total of 398 distance restraints (per SL1Δ dimer) were determined for non-exchangeable protons; these comprised 136 intraresidue and 198 interresidue restraints, as well as 60 restraints involving the unpaired loop adenines. Average flat-well width for interproton distance restraints was 1.57 Å.

The distance restraints extracted from 2D NOE data were supplemented with 108 Watson-Crick hydrogen bonding restraints for the base pairs identified in water 2D NOE spectra. Sugars of all residues except G7, A8 and A9 were restrained as C3′-*endo* due to the absence of H1′-H2′ cross-peaks in dqfCOSY experiments (see below). Glycosidic bond rotations (*chi* angles) were constrained in the '*anti*' range, as only weak base-H1′ cross-peaks were observed in 2D NOE spectra. Backbone torsion angle restraints for A-type geometry were applied to the proximal stem regions (i.e. the first five base pairs) and to the four central base pairs of the palindrome helix; to minimize bias these restraints were given only 1/10th the weighting of experimental distance restraints to avoid any structural bias during DYANA calculations and were subsequently removed altogether during final restraint-energy minimization in AMBER.

2.4. Structural calculations

Initial structures were calculated in the program DYANA, version 1.2, which uses simulated annealing combined with molecular dynamics in torsion angle space [15]. The program was supplied with the set of restraints described above, and simulated annealing was performed with 10 000 steps of torsion angle molecular dynamics. The protocol involved slow cooling from the initial high temperature followed by 2000 steps of conjugate gradient minimization. During the final 200 steps, the van der Waals term was weighted 2.5 times to overcome steric violations. A total of 400 structures were calculated and ranked in order of increasing target function. The 25 structures with the lowest target function and no consistent restraint violations were selected and subjected to further refinements using the AMBER 5.0 force field.

2.5. Structure refinement in AMBER 5.0

It was noted that structures generated by DYANA sometimes included incorrect prochiral centers, perhaps due to a paucity of informative restraints. Energy minimization (500 steps) on each DYANA-generated structure was therefore performed with the belly option in the SANDER module of AMBER 5.0 to fix any incorrect chiralities. Subsequently, 25 structures generated in DYANA were subjected to 10 ps of restrained molecular dynamics (rMD) in AMBER 5.0 using the force field of Cornell et al. [16]. This was an attempt to capture localized dynamics possibly embedded in our NMR restraints, which would not be revealed by energy minimization alone. Hydrated sodium ions were placed against phosphate centers to neutralize the backbone. The rMD protocol began by heating the structure up to 900 K in 1 ps and maintaining high temperature for the next 2 ps while simultaneously increasing restraint weights to 90 kcal mol^{-1} Å^{-2} for distance restraints and 135 kcal mol^{-1} rad^{-2} for torsion angle restraints. After 3 ps equilibration, temperature and force constants were rescaled to 300 K, with 30 kcal mol^{-1} Å^{-2} for distance and 45 kcal mol^{-1} rad^{-2} for angle restraints in 1 ps. Structures were then equilibrated at this level for 6 ps. The van der Waals term of the force field was simultaneously reduced to 0.1 as the temperature was raised to 900 K, increased to 3 during a 1-ps cooling period for 1 ps, and finally brought to 1.0 for the rest of the run. The electrostatic term was switched off for the first 5 ps, and on during the last 5 ps, of each rMD run. Out of 25 initial structures, 15 structures were selected after rMD runs on the bases of final convergence, stability of rMD trajectory, favorable AMBER energies, and residual violations of NMR restraints. The coordinate sets from the last 2 ps of each selected trajectory were averaged and subjected to a final restrained energy minimization of 1000 steps, applying only NMR restraints with a 30 kcal mol^{-1} Å^{-2} force constant.

This final ensemble of structures was subjected to analysis via CORMA, which derives a set of theoretically calculated 2D NOE intensities for a given structure or ensemble of structures and is capable of calculating several indices, such as crystallographic *R* factor and sixth-root *R* factor, to evaluate the quality of structures.

Table 1
Statistics of NMR restraints and parameters for final structural ensemble

a.	Distance and dihedral restraints (per dimer)		
	Total distance restraints		394
		Intraresidue	136
		Interresidue	198
		Interresidue involving flanking adenines	60
	Distance restraints from H_2O data		68
	Average restraints per residue		10
	Torsion angle restraints for sugar puckers		230
	Hydrogen bonding distance restraints		54
	Hydrogen bonding angle restraints		54
	Backbone torsion angle restraints		132
	Total number of restraints		932
b.	Final ensemble statistics		
	Number of structures included		15
	E_{amber}		-4096 ± 251.61 kcal mol^{-1}
	$E_{violations}$		169.2 ± 18.23 kcal mol^{-1}
	Number of distance deviations >0.3 Å		11.4 ± 2.8
	Average deviations from bounds		
		Distance restraint	0.045 ± 0.003 Å
		Angle restraint	$0.598 \pm 0.236°$
		Dihedral angle restraint	$1.848 \pm 0.297°$
	rmsd from ideal geometry		
		Bonds	0.011 ± 0.00019 Å
		Angles	$3.07 \pm 0.130°$
c.	Pairwise all-atom rms deviations		
	All 46 residues		3.30 ± 0.74 Å
	Stem residues		1.11 ± 0.54 Å
	GCGCGC palindrome duplex		1.39 ± 0.45 Å
	Flanking adenine residues		149 ± 0.538 Å

3. Results and discussion

3.1. Resonance assignments

Proton resonance assignments for the SL1Δ dimer were made using a sequential assignment strategy [17]. A complete sequential walk was made in the H1′-base region, starting at the most downfield shifted locations with G1H2′ and intra- and interresidue 2D NOEs for G1H2′-G1H8 and G1H2′-G2H8 proton pairs (Fig. 2). Assignments of H2′ and H3′ protons were unambiguously made using the strong 2D NOEs for interresidue H2′-base, intraresidue H1′-H2′, and intraresidue base-H3′ contacts at a mixing time of 50 ms. At 400 ms mixing time, a sequential H1′-H1′ 2D NOE network was also seen. Assignments for other anomeric protons were confirmed from intraresidue 2D NOEs from H1′ protons. Assignments of H2 protons in adenines were made in two phases: first, resonances in the aromatic region that lacked 2D NOEs for typical anomeric contacts were identified; then, with the help of water-2D NOE data, H2 protons of A4 and A5 residues were identified by the 2D NOEs arising from their expected base-pairing interactions with imino protons of U20 and U21, respectively. These assignments were further confirmed by 2D NOE interactions of AH2 protons with H1′ protons of the following nucleotides on each strand, as well as with H1′ protons across the minor groove on the complementary strand. Also, sequential 2D NOEs were observed for the A4H2-A5H2 proton pairs. In water-2D NOE data, an imino proton network established the presence of Watson-Crick-type hydrogen bonding for the base pairs expected in the helical stem and palindromic regions. The wobble base pair, U6-G18, exhibited its characteristic strong imino-imino contact.

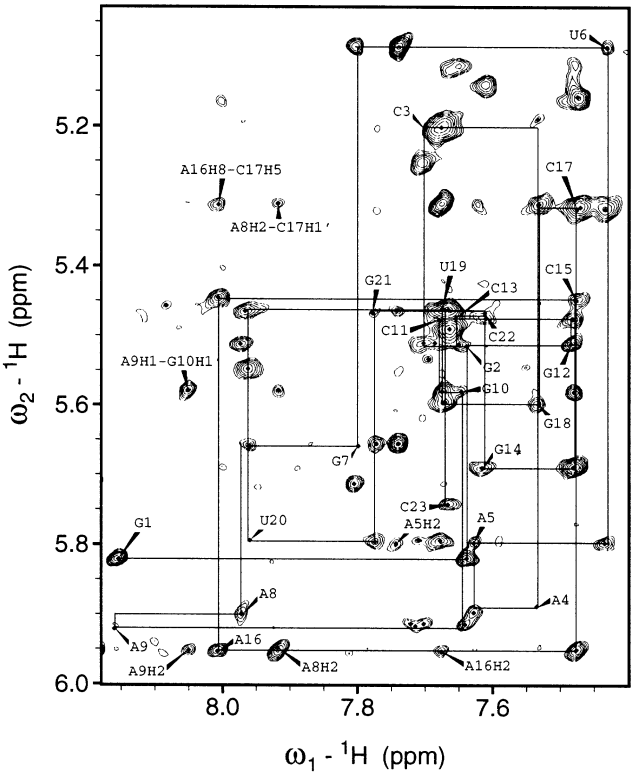

Fig. 2. Sequential walk for base-H1′ resonances in a 400-ms 2D proton NOE spectrum of the SL1Δ mature dimer at 25°C.

The assignments for the loop adenines (A8, A9 and A16) were made sequentially using their interresidue H1′ connectivities. The entire network of connectivities arising from these bases is schematized in Fig. 3. The H2 protons of all three adenines showed cross-peaks to each other, but 2D NOEs for the A8-to-A9 step were noticeably weak. Significantly, the A16H2 proton had NOEs with A8H2 and A9H2 that were of equal intensity, whereas NOEs between A8H2 and A9H2 were much weaker than those between A16H2 and A9H2. This suggested that the A16 residue was positioned between A9 and A8. Further supporting this conclusion were two NOEs between A16H1′ and H2 protons on A8 and A9. In addition, all three adenines were found to have NOEs to their neighboring residues, such as H1′-base NOEs, that are typical of A-type helices. The GCGCGC palindrome also showed NOEs typical of A-type geometry. All sugars were in C3′-*endo* conformation except residues G7, A8, and A9, which showed faint dqfCOSY peaks for H1′-H2′ couplings, an indication of finite conformational flexibility for these sugars. This latter finding further supports the conclusion that A16 is sandwiched between A8 and A9, as this would require local elongation of the backbone, which could be achieved by mixed sugar puckering (see below).

3.2. Generation and refinement of the structural ensemble

Initial structures were generated with DYANA-1.2 using MARDIGRAS to calculate accurate bounds on the experimental distance restraints. Restraint data were supplemented with sugar pucker, hydrogen bonding and backbone torsion angle restraints as described in Section 2.5. A list of structural restraints is presented in Table 1. A total of 400 structures were calculated in DYANA using an annealing protocol. In general, structures selected for further analysis showed no consistent violation of applied restraints, and the 16 individual restraint violations of more than 0.3 Å in the initial ensemble were closely examined. Of these, the maximum violations were 0.89 Å for the A9H2′- G10H1′ contact, and 0.87 Å for U6H2′-G7H8. Note that these violations occurred in only a few structures and that in most structures even these restraints were satisfied. In the end, 25 structures with the lowest target function and no consistent violations were subjected to further refinement using AMBER 5.0.

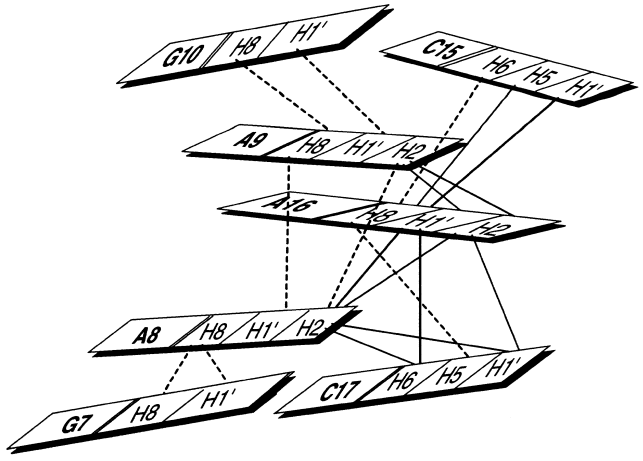

Fig. 3. Schematic representation of 2D NOE contacts involving the loop adenines (A8, A9 and A16) and neighboring bases within each bulge of the mature dimer. Linewidths indicate the relative intensities of the 2D NOE cross-peaks.

rMD was performed on 25 structures following the protocol discussed in Section 2.5. A 10-ps run was found to be adequate to satisfy energetics and restraint violations in refining these structures. After simulated high temperature and force constant treatment, all of the structures tended to converge toward a consensus conformation, with final AMBER energies in the range of -4096 (± 256) kcal mol^{-1} across the ensemble. Residual restraint violations were small and infrequent, indicating that NMR restraints were globally satisfied. Restraints that showed the greatest violations in individual structures were A8H2-A16H1′ (0.34 Å) and A8H2-C17H6 (0.35 Å); the violations apparently reflected a failure to satisfy several conflicting distance restraints, and can best be explained by local conformational flexibility of A8.

Final structures were obtained after averaging over the last 2 ps from rMD trajectories and 1000-step restrained energy minimization using only NMR-derived restraints. The 15 best structures were pooled to create the final structural ensemble, whose coordinates were then averaged and subjected to mild energy minimization to produce a consensus structure. Sixth-root R factors (R_x) were calculated for this ensemble using CORMA [18]. The overall R_x value calculated at 50 ms was 0.041, and the 'interresidue R_x' for the same data was 0.033, both of which indicate excellent agreement with experimental data across the ensemble. Slightly higher values were obtained for the central GCGCGC palindrome alone values (0.055 overall and 0.053 interresidue), or for the flanking adenines (0.046 overall, 0.037 interresidue). Similarly, although the calculated rmsd value for the stem regions alone is only 1.11 Å, those of the palindrome and flanking adenines are somewhat higher, and the global rmsd for the entire duplex is 3.30 Å (Table 1). This likely indicates that, although both stem helices of the duplex are well-defined, local flexibility around the flanking adenines extends into the palindrome helix and contributes to overall flexibility along the length of the duplex, so that individual structures are not strictly superimposable.

3.3. Structure of the linear duplex

The conformation of the mature duplex is that of a roughly linear double helix punctuated by two relatively flexible bulges that each encompass three unpaired adenines (Fig. 4a–c). In contrast to the kissing-loop complex, where the distal G·C base pair of each stem is disrupted, all potential Watson-Crick pairs are intact in the linear duplex. While the stem regions at either end of the duplex have a structure approximating standard A-type helices, the palindromic minihelix, located between the two bulges, is slightly distorted. In particular, although the helical rise and twist values across the palindrome are normal, the G10·C15 base pairs at either end have abnormally high roll values of about 15°, coupled with a positive shift, so that the backbone at the 3′ end of each palindrome is rotated outward and underwound as it approaches A16. As a result, A16 is displaced away from C15 so that the two cannot stack, and A16 instead intercalates between the A8 and A9 bases of the opposite strand (Fig. 4d). Throughout the ensemble, we found that A9 was consistently stacked against A16* (i.e. A16 from the opposite strand), an interaction achieved by displacing A9 slightly inward toward the central axis of the stem helix and rotating it into a plane roughly perpendicular to that of G10. Con-

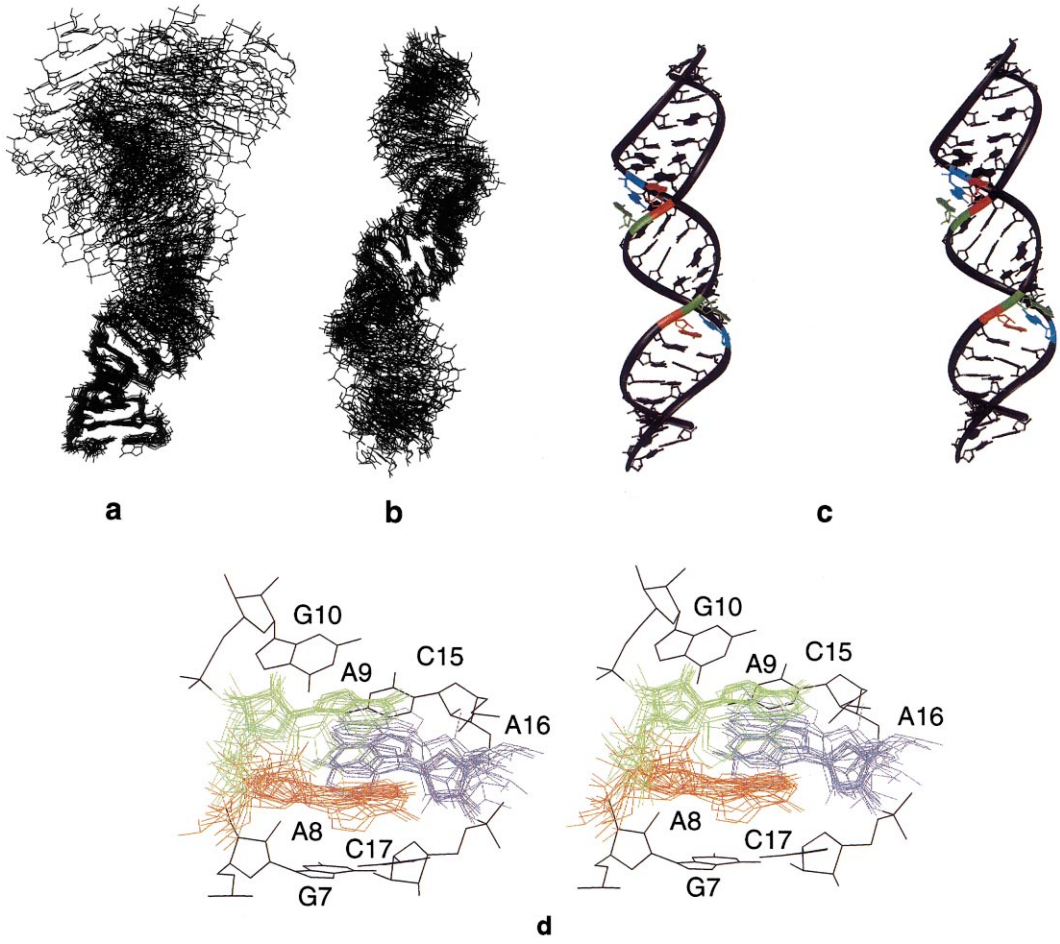

Fig. 4. Structure of the linear dimer of SL1Δ RNA. The same final ensemble of 15 structures is shown superimposed with respect to either (a) one stem region or (b) the central GCGCGC palindrome duplex. Only heavy atoms are shown. c: A stereoview of the average structure generated from this ensemble. The loop adenines are depicted in orange (A8), green (A9) and blue (A16). d: Stereoview of one bulge region of the dimer. Complete ensembles for A8, A9 and A16 are presented, colored as in panel c. Average locations of the adjacent G7·C17 and G10·C15 base pairs are also shown.

versely, A8 was displaced slightly outward and, though it remained stacked against G7, contacted A16* at an angle that allowed only partial stacking (Fig. 4d). Thus, rather than forming a single colinear stack of sequential bases as it would in a conventional double helix, each RNA strand in this structure is distorted by the intercalation of A16* between A8 and A9, by partial discontinuity of stacking between A8 and A16*, and by complete discontinuities between A9 and G10 and between C15 and C17.

3.4. Comparison to the kissing-loop dimer

Despite their divergent global structures, the 2D proton NMR spectra of the mature dimer were remarkably similar to those of its kissing-loop isomer, which we described previously [10]. This is to be expected, as the local environments and bonding interactions of most individual bases are similar in both structures, except that all intramolecular base pairs of the kissing dimer are converted to homologous intermolecular pairs during maturation. One salient difference is that the G7·C17 base pair predicted to exist in the SL1 monomer (Fig. 1) is present in the mature dimer (Fig. 4c,d) but unequivocally absent from the kissing-loop form [10]. Rupture of this base pair in the kissing dimer appears to result from local mechanical strains imposed by an unusual pattern of intermolecular stacking of the A9 bases which does not persist in the linear duplex. To form the kissing dimer, each A9 base must flip out around the backbone to stack against bases of the opposite strand, a rotation that requires *trans* rotation across its backbone *alpha* angle [10]; this is apparent in the 1D ^{31}P NMR spectrum of the kissing dimer, which shows upfield-shifted phosphorus resonances that reflect the unusual backbone conformation (Fig. 5). In the linear dimer, by contrast, although the A16 bases are displaced between strands, no unusual shifts are seen in the phosphorus spectrum (Fig. 5), indicating that all backbone angles are within the range observed for a standard double helix, which implies less mechanical distortion in the mature form. The mechanical strains in the kissing-loop dimer also result in marked flexion and elongation of the palindrome minihelix, manifested by high positive roll values between all six of its base pairs [10]; by contrast, only the two outer (G10·C15) pairs show high roll values in the linear dimer. In addition, the nearly linear strand conformations in the mature duplex allow more continuous stacking, leaving fewer bases exposed to solvent water than in the kissing dimer. Together, the favorable thermodynamic effects of reforming the G7·C17 base pair, increasing stacking,

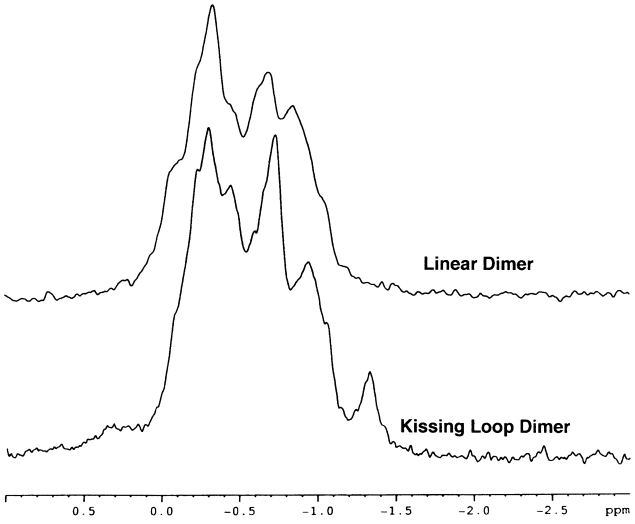

Fig. 5. Comparison of 1D ^{31}P NMR spectra for the mature linear (above) and kissing-loop (below) dimers of SL1Δ RNA.

and relieving mechanical strain across the palindrome helix likely account in large measure for the tendency of the kissing-loop complex to refold spontaneously into linear form.

3.5. Comparison to a recently published structure

In a recent report, Girard et al. [11] have published the NMR solution structure of a similar linear RNA duplex formed by a truncated SL1 sequence. Though the RNAs we examined differ somewhat in the sequence of the SL1 stem, the structures we obtained are in excellent agreement and strongly confirm one another. The only notable disparity is in the degree of convergence among elements making up the two structural ensembles: whereas Girard et al. present a surprisingly tight ensemble (rmsd 0.9 Å overall and 0.36 Å for the palindrome alone), ours depicts a more flexible molecule in which the three helical segments are each well defined (rmsd 1.1–1.4 Å) but exhibit hinge-like motion with respect to one another, making it difficult to superimpose all regions simultaneously (cf. Figs. 4a and 4b) and yielding an overall rmsd of 3.3 Å. As hinge-like motion is typical at bulges in RNA duplexes [19,20], we suggest that the apparent flexibility we observe is an authentic property of the mature SL1 dimer.

4. Conclusions

The SL1 sequence of HIV-1 RNA can adopt two alternative dimer structures: a kissing loop complex, and a bulged linear duplex. Although each can be maintained stably under appropriate conditions, the kissing complex has a marked tendency to isomerize into linear form both in vitro and in the virus, suggesting that it represents a transient folding intermediate. The structures of both dimers have now been solved using NMR ([10,11], and the present report), and they shed light on the disparate thermodynamic stabilities of the two forms. Specifically, the dimer gains stability through reformation of a ruptured base pair, through increased linear base stacking, and through a decrease in mechanical strain as it isomerizes from kissing loop to mature form. The precise sequence of events that occur during maturation remains to be determined, as does the mechanism by which the HIV-1 nucleocapsid protein catalyzes the refolding process.

Acknowledgements: We thank Markus W. Germann (Thomas Jefferson University) for assistance with ^{31}P NMR. Use of the UCSF Computer Graphics Laboratory is gratefully acknowledged. This work was supported in part by NIH Grant AI36636.

References

[1] Berkowitz, R., Fisher, J. and Goff, S.P. (1996) Curr. Top. Microbiol. Immunol. 214, 177–218.
[2] Haddrick, M., Lear, A.L., Cann, A.J. and Heaphy, S. (1996) J. Mol. Biol. 259, 58–68.
[3] Paillart, J.C., Berthoux, L., Ottman, M., Darlix, J.L., Marquet, R., Ehresmann, B. and Ehresmann, C. (1996) J. Virol. 70, 8348–8354.
[4] Clever, J.L. and Parslow, T.G. (1997) J. Virol. 71, 3407–3414.
[5] Laughrea, M. and Jette, L. (1994) Biochemistry 33, 13464–13474.
[6] Marquet, R., Paillart, J.C., Skripkin, E., Ehresmann, C. and Ehresmann, B. (1994) Nucleic Acids Res. 22, 145–151.
[7] Clever, J.L., Wong, M.L. and Parslow, T.G. (1996) J. Virol. 70, 5902–5908.
[8] Darlix, J.L., Gabus, C., Nugeyre, M.T., Clavel, F. and Barre, S.F. (1990) J. Mol. Biol. 216, 689–699.
[9] Clever, J.L., Sassetti, C. and Parslow, T.G. (1995) J. Virol. 69, 2101–2109.
[10] Mujeeb, A., Clever, J.L., Billeci, T.M., James, T.L. and Parslow, T.G. (1998) Nature Struct. Biol. 5, 432–436.
[11] Girard, F., Barbault, F., Gouyette, Huynh-Dinh, T., Paoletti, J. and Lancelot, G. (1999) J. Biomol. Struct. Dyn. 16, 1145–1157.
[12] Liu, H., Borgias, B., Kumar, A. and James, T.L. (1990, 1994) MARDIGRAS, University of California, San Francisco, CA.
[13] Liu, H., Spielmann, H.P., Ulyanov, N.B., Wemmer, D.E. and James, T.L. (1995) J. Biomol. NMR 6, 390–402.
[14] Liu, H., Tonelli, M. and James, T.L. (1996) J. Magn. Reson. 111, 85–89.
[15] Güntert, P., Mumenthaler, C. and Wüthrich, K. (1997) J. Mol. Biol. 273, 283–298.
[16] Cornell, W., Cieplak, P., Bayly, C.I., Gould, I.R. and Kollman, P.A. (1996) J. Am. Chem. Soc. 118, 2309–2309.
[17] Varani, G. and Tinoco Jr., I. (1991) Q. Rev. Biophys. 24, 479–532.
[18] Keepers, J.W. and James, T.L. (1984) J. Magn. Reson. 57, 404–426.
[19] Lee, A.J. and Crothers, D.M. (1998) Structure 6, 993–1005.
[20] Diener, J.L. and Moore, P.B. (1998) Mol. Cell 1, 883–894.